mon petrogenetic process was involved in hawaiite formation. This most likely involved interaction between an enriched component with a high Rb/Sr ratio and low Sm/Nd ratio and a depleted component with a lower Rb/Sr ratio and higher Sm/Nd ratio.

We used the same methodology (Table 1 and Figs. 2 and 3) to identify the sources of all 19 adzes. In addition to the adzes from Kaho'olawe, Hawai'i (n = 1); the Pitcairn Group (n = 1), and Rurutu (n = 1), adzes were also identified that were manufactured from basalt sources on Eiao in the Marquesas (n = 1); Rapa in the Australs (n = 1); the Society Islands with Ba/Th ratios >100, such as Ra'iatea, Taha'a, or Huahine (n = 7); and the Society Islands with Ba/Th ratios <100, such as Tahiti (n = 7).

Because adze C7727 was collected from Napuka, a low coral atoll in the western Tuamotus in central East Polynesia (Fig. 1B), the rock from which it was made was transported a minimum distance of 4040 km from its source on Kaho'olawe in the Hawaiian chain (Fig. 1A). The likely route between Hawai'i and Tahiti via the Tuamotus (*35*) (Fig. 1A) has favorable winds and currents for two-way voyages. Experimental canoes using non-instrumental navigation made such a journey in 32 days (*36*).

There is much traditional ceremony in preparation for long-distance voyaging, and today, as possibly in the ancient past, canoeists often stop at the westernmost tip of Kaho'olawe Island, Lae o Kealaikahiki (literally, "cape or headland of the way to Tahiti") (Fig. 1C) before beginning their voyage south. Sample C7727, a Duff type 3A adze, is made from rock that is consistent with hawaiite deposits found at only a few places along the coast of this island, one of which is close to Lae o Kealaikahiki. This adze type is unknown from Hawai'i but is common in the Tuamotus. Rock from Kaho'olawe may thus have been taken as a gift or memento (as is done today by modern traditional voyagers) or used as ballast, and fashioned into adzes in the Tuamotus.

The Tuamotus, along with the Society Islands, could be approached from all quarters and was thus probably important in Polynesian trade (*2*). Our data show that Tuamotu adzes originate from the Marquesas, Pitcaim, Austral, and Society Islands; that is, most of the island groups surrounding the atoll archipelago. Furthermore, because the low coral atolls of the Tuamotus emerged after 1200 CE (*37*), and the surrounding island groups were colonized well before then, all imported adzes recovered in the Tuamotus relate to postcolonization interaction with adjacent archipelagoes. We therefore agree with Irwin (*2*) that postcolonization voyaging must have been common enough for voyaging knowledge to be passed across generations and that it continued until about 1450 CE when most voyaging ceased in East Polynesia (*38*).

References and Notes

1. A. Sharp, *Ancient Voyages in Polynesia* (Univ. of California Press, Berkeley, CA, 1964).
2. G. Irwin, *The Prehistoric Exploration and Colonisation of the Pacific* (Cambridge Univ. Press, Cambridge, 1992).
3. M. Levison, R. Ward, J. Webb, *The Settlement of Polynesia: A Computer Simulation* (Univ. of Minnesota Press, Minneapolis, MN, 1973).
4. B. R. Finney, *Science* **196**, 1277 (1977).
5. P. V. Kirch, *On the Road of the Winds: An Archaeological History of the Pacific Islands before European Contact* (Univ. of California Press, Berkeley, CA, 2000).
6. G. Irwin, *J. Polynesian Soc.* **107**, 111 (1998).
7. C. K. Cachola-Abad, *N. Z. Archaeol. Assoc. Mon.* **19**, 13 (1993).
8. Details are found in the supporting material on *Science* Online.
9. S. Best, P. Sheppard, R. Green, R. Parker, *J. Polynesian Soc.* **101**, 45 (1992).
10. M. I. Weisler, *N. Z. Archaeol. Assoc. Mon.* **21** (1997).
11. A. W. Hofmann, *Nature* **385**, 219 (1997).
12. T. L. Grove, N. Chatterjee, S. W. Parman, E. Medard, *Earth Planet. Sci. Lett.* **249**, 74 (2006).
13. T. L. Grove *et al.*, *Contrib. Mineral. Petrol.* **145**, 515 (2003).
14. Y. L. Niu, M. J. O'Hara, *J. Geophys. Res. Solid Earth* **108**, 2209 (2003).
15. W. J. Morgan, *Am. Assoc. Petrol. Geol. Bull.* **56**, 203 (1972).
16. J. A. Tarduno *et al.*, *Science* **301**, 1064 (2003).
17. A. Bonneville, L. Dosso, A. Hildenbrand, *Earth Planet. Sci. Lett.* **244**, 251 (2006).
18. J. A. Pearce, J. R. Cann, *Earth Planet. Sci. Lett.* **19**, 290 (1973).
19. C. Hemond, C. W. Devey, C. Chauvel, *Chem. Geol.* **115**, 7 (1994).
20. J. A. Pfander, C. Munker, A. Stracke, K. Mezger, *Earth Planet. Sci. Lett.* **254**, 158 (2007).
21. A. Zindler, S. Hart, *Annu. Rev. Earth Planet. Sci.* **14**, 493 (1986).
22. K. P. Emory, *Material Culture of the Tuamotu Archipelago* (Pacific Anthropological Records 22, Bishop Museum, Honolulu, HI, 1975).
23. R. Duff, in *Anthropology in the South Seas*, J. D. Freeman, W. R. Geddes, Eds. (Thomas Avery & Sons, New Plymouth, New Zealand, 1959), pp. 121–147.
24. W. P. Leeman, D. C. Gerlach, M. O. Garcia, H. B. West, *Contrib. Mineral. Petrol.* **116**, 62 (1994).
25. A. R. Basu, B. E. J. Faggart, in *Earth Processes: Reading the Isotopic Code*, A. Basu, S. Hart, Eds. (American Geophysical Union, Washington, DC, 1996), pp. 149–159.
26. S. C. Huang *et al.*, *Geochem. Geophys. Geosyst.* **6**, Q01L06 (2005).
27. W. Abouchami *et al.*, *Nature* **434**, 851 (2005).
28. G. Xu *et al.*, *Geochem. Geophys. Geosyst.* **8**, 10.1029/2006GC001554 (2007).
29. C. Y. Chen, F. A. Frey, M. O. Garcia, *Contrib. Mineral. Petrol.* **105**, 197 (1990).
30. H. B. West, W. P. Leeman, *Earth Planet. Sci. Lett.* **84**, 211 (1987).
31. R. V. Fodor, F. A. Frey, G. R. Bauer, D. A. Clague, *Contrib. Mineral. Petrol.* **110**, 442 (1992).
32. F. A. Frey *et al.*, *J. Geophys. Res. Solid Earth* **95**, 1271 (1990).
33. A. W. Hofmann, K. P. Jochum, *J. Geophys. Res. Solid Earth* **101**, 11831 (1996).
34. W. M. White, R. A. Duncan, in *Earth Processes: Reading the Isotopic Code*, A. Basu, S. Hart, Eds. (American Geophysical Union, Washington, DC, 1996), pp. 183–206.
35. B. R. Finney, in *Polynesian Culture History, Essays in Honor of Kenneth P. Emory*, G. A. Highland, R. W. Force, A. Howard, M. Kelly, Y. H. Sinoto, Eds. (Bishop Museum Press, Honolulu, HI, 1967), pp. 141–166.
36. B. R. Finney, *Voyage of Discovery, A Cultural Odyssey through Polynesia* (Univ. of California Press, Berkeley, CA, 1994).
37. W. R. Dickinson, *Palaeogeogr. Palaeoclimatol. Palaeoecol.* **213**, 251 (2004).
38. M. I. Weisler, in *Geochemical Evidence for Long-Distance Exchange*, M. D. Glascock, Ed. (Bergin & Garvey, London, 2002), pp. 257–273.
39. J. H. Chen, G. J. Wasserburg, *Conf. Abstr. Lunar Planet. Inst.* **1**, 103 (1983).
40. R. Brousse, T. Gisbert, C. Leotot, *C. R. Acad. Sci. Ser. 11* **303**, 247 (1986).
41. W. White, personal communication.
42. Unpublished data are from Rice University, MPI Mainz, and Washington State University (W. P. Leeman, personal communication).

43. Y. Sinoto and B. Kam gave permission to core adzes from the Bishop Museum, Hawai'i. Access to the Hawai'i Institute for Geophysics for coring the adzes was facilitated by J. Sinton and R. Bollt. Data used to locate the hawaiite source of C7727 on Kaho'olawe were provided by S. Huang and W. P. Leeman.

Supporting Online Material

www.sciencemag.org/cgi/content/full/317/5846/1907/DC1
Materials and Methods
SOM Text
Figs. S1 to S7
Tables S1 to S5
References

26 June 2007; accepted 28 August 2007
10.1126/science.1147013

Synchrony Dynamics During Initiation, Failure, and Rescue of the Segmentation Clock

Ingmar H. Riedel-Kruse,*† Claudia Müller, Andrew C. Oates†

The "segmentation clock" is thought to coordinate sequential segmentation of the body axis in vertebrate embryos. This clock comprises a multicellular genetic network of synchronized oscillators, coupled by intercellular Delta-Notch signaling. How this synchrony is established and how its loss determines the position of segmentation defects in Delta and Notch mutants are unknown. We analyzed the clock's synchrony dynamics by varying strength and timing of Notch coupling in zebrafish embryos with techniques for quantitative perturbation of gene function. We developed a physical theory based on coupled phase oscillators explaining the observed onset and rescue of segmentation defects, the clock's robustness against developmental noise, and a critical point beyond which synchrony decays. We conclude that synchrony among these genetic oscillators can be established by simultaneous initiation and self-organization and that the segmentation defect position is determined by the difference between coupling strength and noise.

The periodic and sequential segmentation of the vertebrate embryo along its anterior-posterior axis into blocks of cells called somites, the precursors of axial bone and muscle, is thought to be driven by the segmentation clock (Fig. 1A) (*1*, *2*). This clock com-

prises a multicellular genetic network of oscillators located within the posterior mesoderm (Fig. 1B) (*3*, *4*). Delta-Notch signaling has been proposed (*3*, *5*) to couple these oscillators (Fig. 1C) such that they are spatiotemporally synchronized despite the presence of noise. Desynchronization over developmental time (*5*) could explain the zebrafish Delta-Notch mutant phenotypes (*6*–*10*) in which only the first 6 to 10 anterior segments form correctly (*11*); alternatively, genetic differences in anterior and posterior patterning might set the positions of these segmentation defects (*11*, *12*). A physical theory that accounts for these defect positions based on desynchronization dynamics and Delta-Notch signaling strength is lacking, and how this clock is started and attains initial synchrony is also unknown.

If desynchronization is the cause of Delta-Notch mutant phenotypes, such a decay process should be inducible throughout somitogenesis. We delivered saturating doses of N-[N-(3,5-difluorophenacetyl-L-alanyl)]-S-phenylglycine t-butyl ester (DAPT) to wild-type (WT) embryos at hourly intervals (*13*). DAPT binds to and blocks the intramembrane protease required for cleavage of the Notch intracellular domain in response to Delta binding the receptor's extracellular domain (Fig. 1D) (*14*). We quantified the resulting organismal phenotype with the anterior limit of defects (ALD) (Fig. 1E), that is, the number of the anterior-most defective segment (*15*), which, averaged over an embryo population, is characteristic for each mutant (*11*, *15*) and is indicated by the myotome boundary marker cb1045 (*16*). The ALD of fixed embryos translated into the developmental time, t, of the first misformed segment boundary (Fig. 1F) because segments formed at a linear rate

$$S = \alpha \cdot t - \mu \qquad (1)$$

with segment number S, segmentation rate α = 2.5 ± 0.25 hour^{-1}, and offset μ = 25 ± 3 (N = 6 embryos) (mean ± uncertainty = 2 SEM and 95% confidence unless stated otherwise). DAPT delivered before t_0 = 5.8 ± 0.5 hours caused a constant ALD of $S_{ALD}^{-/-}$ = 5.2 ± 0.18 (N = 31), whereas later delivery shifted the ALD posteriorly (Fig. 1, E and F). These data are consistent with a decay process underlying the Delta-Notch mutant phenotype, and, assuming near-instantaneous action of DAPT treatment, t_0 would mark the beginning of this process with a decay time of 6.5 hours.

Furthermore, if desynchronization is the cause of Delta-Notch phenotypes, this decay time should be modifiable. We blocked Notch signaling before t_0 in WT and *des*$^{+/-}$ (*notch1a* heterozygote mutant) (*7*), varying (i) DAPT concentrations to reduce Notch activation and (ii) antisense morpholino (MO) amounts to reduce translation of *notch1a* mRNA (Fig. 1D) (*7*, *13*). Both treatments for quantitative perturbation of gene function gave consistent results (Fig. 2, A and B): The ALD shifted posteriorly with lower treatment levels, and curves for *des*$^{+/-}$ and WT shifted along the treatment axis, requiring about half the amount of treatment in *des*$^{+/-}$ to achieve the same effect as WT, suggesting a 0.5-fold difference in signaling. Saturating MO amounts caused an ALD consistent with *des*$^{-/-}$, $S_{ALD}^{-/-}$ = 7.63 ± 0.12 (N = 108) (*11*), whereas saturated DAPT concentrations caused lower ALDs, as above (Fig. 1, E and F), potentially because of DAPT targeting additional Notch receptors (*17*). Consequently, intercellular Delta-Notch signaling here is not simply a qualitative on-or-off switch; instead it can transmit smoothly graded quantitative signals, and this signal strength sets the decay time.

We sought a physical theory describing the dynamics of synchrony in the segmentation clock that predicts the first defective segment boundary S_{ALD} (=ALD) from the treatment level, n. We consider the segmentation clock as a population of identical, mutually coupled phase oscillators in the presence of noise (*13*, *18*), thereby neglecting the spatial aspects of cyclic gene wave patterns (*2*, *4*) and the biochemical details and amplitudes of the postulated cell-autonomous Her-feedback oscillators (*19*). We then described the synchrony among oscillating cells in mean-field approximation (Fig. 2C) (*13*) by an order parameter Z, with Z = 0 and Z = 1 for none and perfect synchrony, respectively (*18*). Below the threshold Z_c, proper segment formation fails (Fig. 2D). The dynamics of Z approximate an exponential (*18*) starting at t_0

$$Z(t) = Z(t_0) \cdot e^{-\lambda(t-t_0)/2} \qquad (2)$$

with the time constant

$$\lambda = 2\sigma^2 - \varepsilon \qquad (3)$$

determined by the antagonistic influence of the total noise experienced by the clock, $2\sigma^2$, and coupling among cells, ε. $2\sigma^2$ comprises environmental sources, like temperature fluctuations; intracellular sources, like cell division (*3*–*5*); and intercellular sources, like relative cell movements in the PSM mixing cells from regions with different phases (*5*). ε depends linearly on activated Notch protein level, p

$$\varepsilon = \beta \cdot \bar{p} + A \qquad (4)$$

where A accounts for potential additional coupling pathways. The sign of λ then determines whether synchrony decays or builds up, depending on whether noise or coupling dominates, respectively, and its magnitude determines the duration of either process. Hence at λ = 0 the collective behavior of these coupled oscillators undergoes a dramatic qualitative change, which marks the critical point at a synchronization phase transition (*18*, *20*, *21*), analogous to the freezing point at the water-ice transition (*13*).

A Hill equation accounts for the inhibitory effect of treatment level, n, with MO and DAPT assumed to act noncooperatively

$$\bar{p} = \delta \cdot \bar{p}_{WT} \cdot \left(1 - \frac{n}{n + n_0}\right) \qquad (5)$$

and where 2δ = [0, 1, 2] is the number of *notch1a* alleles per embryo, $\bar{p}_{WT}$ is the WT level of activated protein, and n_0 is the treatment level that halves $\bar{p}_{WT}$. When applied to WT, n_0 would then correspond to the heterozygous condition.

Combining Eqs. 1 to 5 yields an expression that predicts the ALD of the homozygous mutant

$$S_{ALD}^{-/-} = (\alpha \cdot t_0 - \mu) - 2 \cdot \alpha \cdot \ln[Z_c/Z(t_0)]/(2\sigma^2 - A) \qquad (6)$$

which is set by the shortest decay time determined by the noise in the system to desynchronize cells in the absence of Notch signaling. More generally, we find the desired expression that predicts the ALD for any reduced Notch coupling strength due to the treatment level, n

$$S_{ALD} = \frac{S_{ALD}^{-/-} \cdot (n + n_0) - (\alpha \cdot t_0 - \mu) \cdot (n_{c,\delta} + n_0)}{n - n_{c,\delta}} \qquad (7)$$

Below the critical treatment

$$n_{c,\delta} = n_0 \cdot (\delta \cdot R - 1) \qquad (8)$$

in principle infinitely many correct segments could be formed. Here we define

$$R = \beta \cdot \bar{p}_{WT}/(2\sigma^2 - A) = \varepsilon_{WT}/(2\sigma^2 - A) \qquad (9)$$

as the robustness (*22*) of segmentation against changes in Notch signaling, other potential coupling pathways, and noise; a three-way balance that quantifies, for instance, the fold reduction in Notch signaling that is tolerable (*13*).

Fitting Eq. 7 to the data (Fig. 2, A and B) and with $S_{ALD}^{-/-}$ and t_0 fixed as above, we found the fit parameters for DAPT of R = 8.6 ± 2.2 and n_0 = 0.66 ± 0.18 μM and for MO, R = 2.1 ± 0.34 and n_0 = 0.021 ± 0.005 pmol; the resulting critical treatment levels, $n_{c,\delta}$, are marked in Fig. 2, A and B. Both values for R are larger than 2, hence consistent with the absence of a segmentation phenotype in the heterozygous mutant. These results provide quantitative evidence for (i) Notch signaling as a coupling mechanism, (ii) desynchronization as the cause of the Delta-Notch mutant phenotype, (iii) the system's robustness of $R \sim 5$, and (iv) the

Max Planck Institute of Molecular Cell Biology and Genetics (MPI-CBG), Pfotenhauerstrasse 108, 01307 Dresden, Germany.

*Present address: Division of Biology, California Institute of Technology, MC 139-74, Pasadena, CA 91125, USA.

†To whom correspondence should be addressed. E-mail: ingmar@caltech.edu (I.H.R.-K.); oates@mpi-cbg.de (A.C.O.)

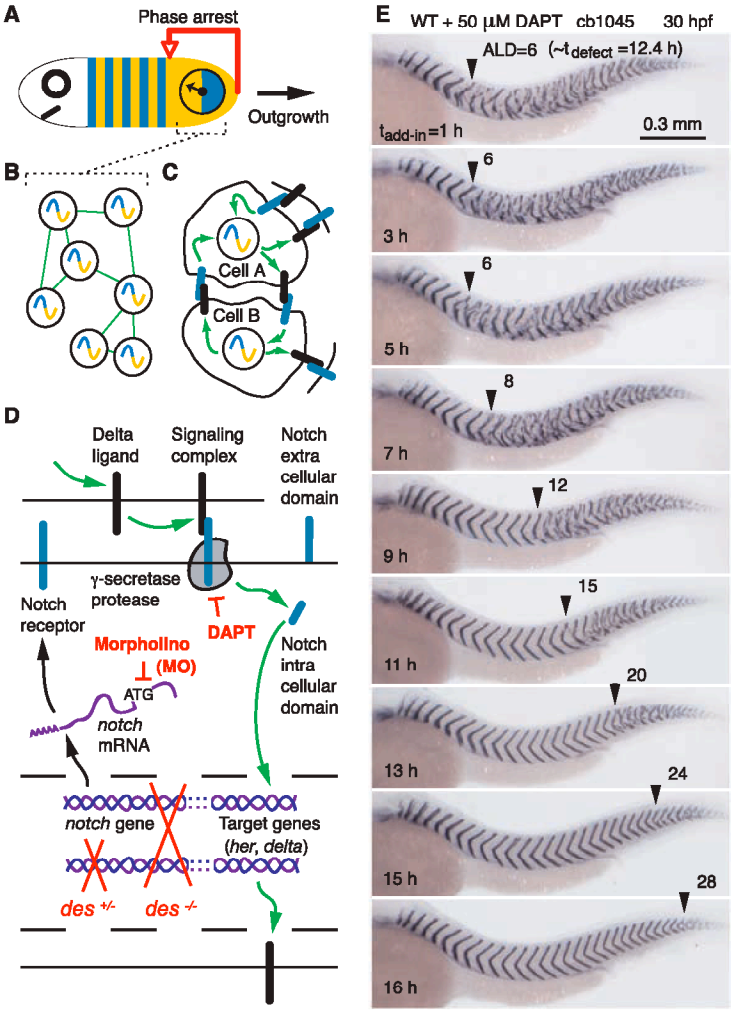

Fig. 1. A decay process within the segmentation clock underlies the Delta-Notch mutant segmentation phenotype. (**A**) Oscillation phase of the zebrafish segmentation clock (blue-yellow) in the outgrowing PSM is continuously imprinted at constant distance from the posterior end via a signaling gradient (*32*), providing cues for successive morphological body segmentation along the anterior-posterior axis. Perturbations in this pattern, i.e., insufficient coherence among oscillators, result in defective segment boundaries. (**B**) Network of genetic oscillators within PSM. (**C**) Mutual coupling via Delta-Notch signaling (green, signal transduction). Coupling acts to decrease phase differences between oscillators and opposes the phase-randomizing effects of noise. (**D**) Production, activation, turnover, and signaling of this pathway (*33*); treatments used in this study to reduce or completely block intercellular Delta-Notch coupling (red): MO, DAPT, and mutants in *notch1a* ($des^{+/-}$ and $des^{-/-}$). (**E**) Shifts in ALD of segment boundaries (arrowheads) from adding saturating DAPT levels at successively later times. (**F**) Functional representation of (E). Morphological ALD (left axis) converts into absolute time of defect (right axis). ALD error bars, ≥68% of scored embryos; solid line, linear fit; dashed lines, visual guidance marking saturating ALD, $S^{-/-}_{ALD}$, and decay onset time, t_0.

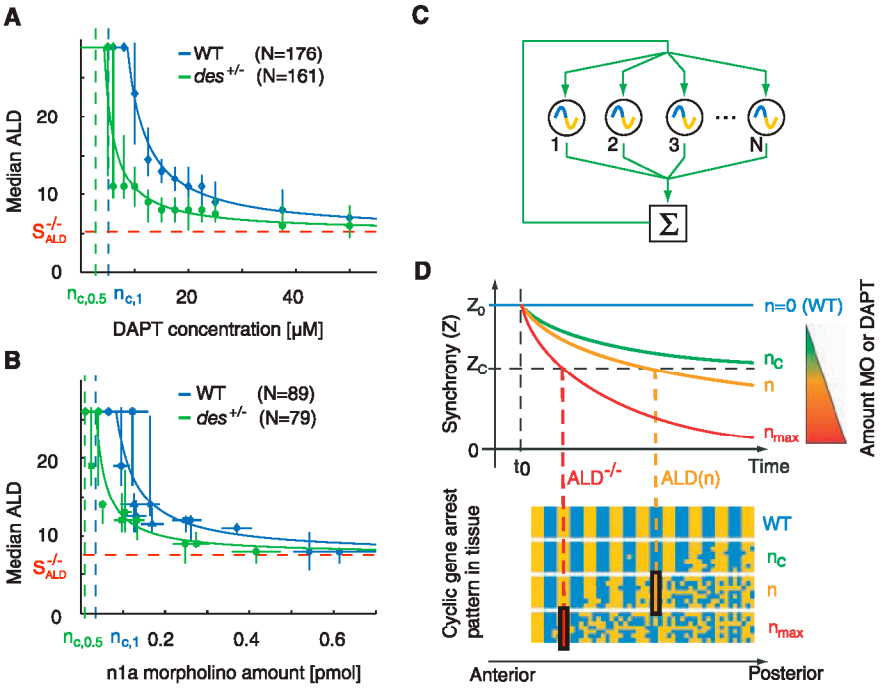

Fig. 2. A mean-field theory of coupled phase oscillators predicts the synchrony decay time in the segmentation clock and the segmentation defect position. (**A**) ALD resulting from various DAPT concentrations applied at dome stage to WT (blue) and $des^{+/-}$ (green). ALD error bars, ≥68% of scored embryos; solid lines, fits to Eq. 7; dashed lines, visual guidance marking saturating ALD, $S^{-/-}_{ALD}$, and critical treatment levels, $n_{c,\delta}$. (**B**) As in (A) but for MO. Concentration error bars, 2 SD. (**C**) Mean-field approximation, where each cell averages over the oscillation phases of all other cells, neglects amplitudes and spatial features of cyclic wave patterns. (**D**) Synchrony among cells, described by order parameter Z (top) or cyclic gene arrest pattern (bottom), decays over time with rate depending on treatment strength, n; below threshold Z_c, segment boundaries are defective, causing an ALD.

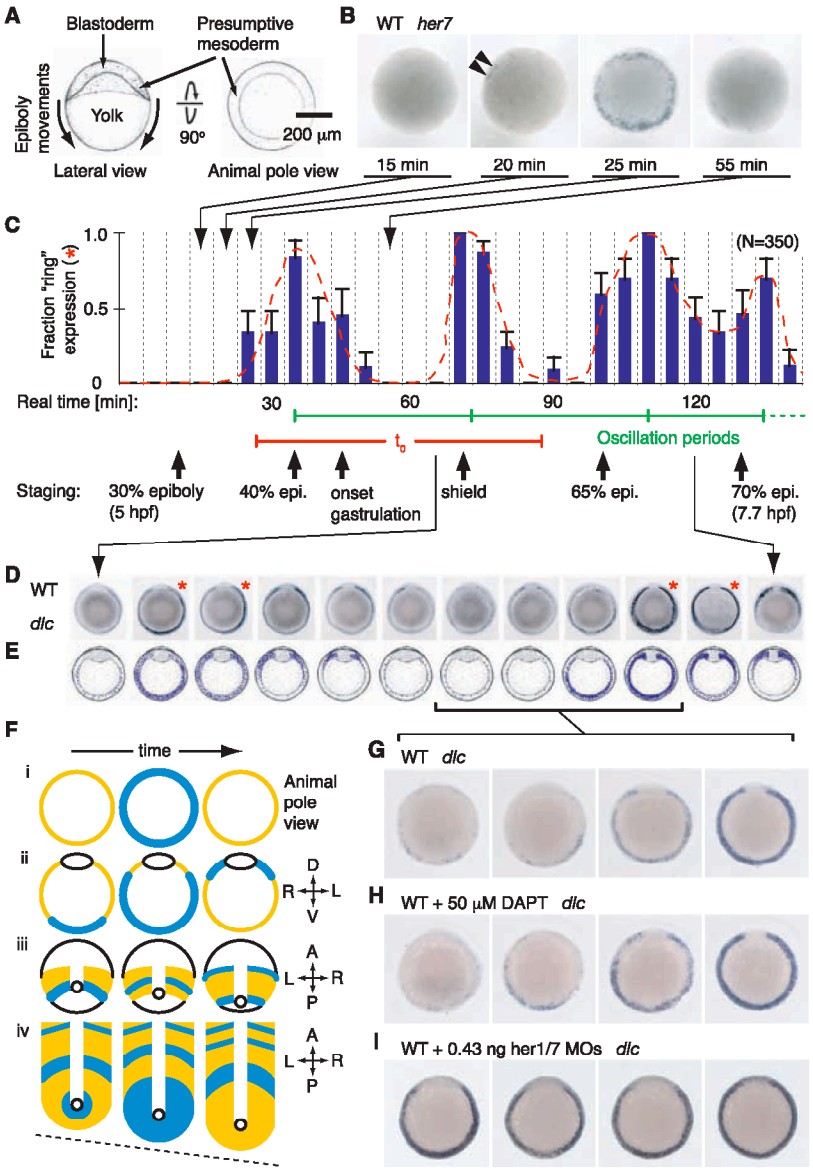

Fig. 3. The genetic oscillators of the segmentation clock are initiated synchronously in a Delta-Notch-independent manner. (**A**) Schematic of late zebrafish blastula stage immediately before mesoderm induction. (**B**) First detection (arrowheads) and first cycle of *her7* expression in presumptive mesoderm ring (animal pole view). (**C**) Temporal distribution of presomitogenesis cyclic gene oscillations; embryos scored for continuous "ring"-shaped expression [red asterisks in (D)] of *dlc* in early mesoderm. Red bar, estimated uncertainty for t_0 when desynchronization starts; error bars, 1 SEM. Red dashed line is for visual guidance. (**D**) *dlc* expression in representative embryos (vegetal view, dorsal to top). (**E**) Illustration of (D) with waves traveling around margin from ventral to dorsal. (**F**) Schematic of changes in cyclic gene expression patterns during different developmental stages: (i) cycle 1 during pregastrula, (ii) cycles 2 to 4 during early gastrula with dorsal side marked, (iii) cycles 5 and 6 during late epiboly with notochord primordium, and (iv) cycles 7 to 30+ during somitogenesis stages with tailbud. (**G** to **I**) Representative sibling embryos, laid over 20 min, showing oscillatory *dlc* expression after dimethyl sulfoxide (DMSO) carrier treatment (G) and DAPT treatment (H), but elevated, stable expression after MO targeting both *her1* and *her7* bHLH repressor protein mRNA (I).

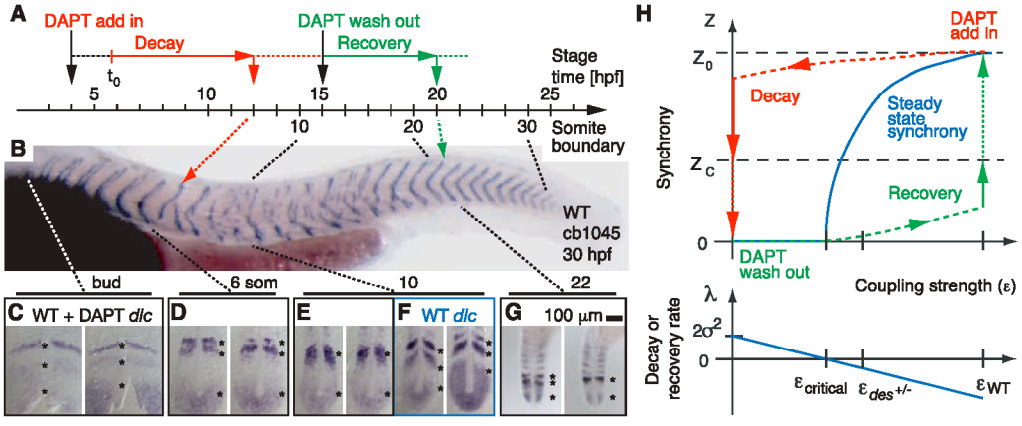

Fig. 4. Delta-Notch coupling is sufficient for self-organized resynchronization of the segmentation clock and rescue of morphological segmentation defects. (**A**) Timeline of DAPT pulse-chase experiment. (**B**) Six anterior segments formed correctly (S_{ALD} = 7), followed by ~15 disrupted segments (red bracket), followed by normally shaped segments posterior to 21st segment (S_{PLD} = 21). Control embryos in DMSO showed no defect phenotype (*14*); embryos remaining in DAPT showed no rescue (Fig. 1E). (**C** to **G**) Representative *dlc* PSM expression patterns, time points marked referring to (B). Two representative embryos showing transition from mildly affected cyclic expression stripes (C), degrading gradually (D) to typical salt-and-pepper pattern indicating desynchronization among cells (E) compared to expected WT pattern (F), and return of normal, symmetrical cyclic gene expression pattern (G). Asterisks mark *dlc* cyclic stripes [(C), (F), and (G)] or disordered expression domains [(D) and (E)]. (**H**) Schematic synchrony-coupling phase diagram (top) and decay or recovery rate-coupling dependency (bottom). Potential additional coupling pathways are neglected for simplicity (A = 0); axes not to scale.

existence of a synchronization transition in a population of biological genetic oscillators (*18*, *20*, *21*).

More generally, the analysis of other complex developing systems (*23*) would be amenable to the quantitative strategy used here. In particular, quantitative MO delivery can be interpreted as a tool to speed up mRNA decay with expected in vivo MO-mRNA binding rates of $K_b \sim 10^4\ M^{-1}\ s^{-1}$ (*13*). Consequently, molecular parameters can be estimated, such as the *notch1a* mRNA decay rate, $k_d \sim 0.1\ min^{-1}$ (*13*).

The onset of desynchronization (Fig. 1F) predicts the clock's initiation at or before $t_0 = 5.8 \pm 0.5$ hours. Around this developmental time point, the cells of the zebrafish presumptive mesoderm that will later become the somites are found in a marginal ring of the blastoderm; epiboly movements will subsequently draw the blastoderm over the yolk (Fig. 3A). We observed the earliest expression of cyclic genes *her1*, *her7*, and *dlc* at ~5.25 hours postfertilization (hpf): 10 min elapsed between first detection of scattered *her7*-positive nuclei and a subsequent ring of expression around the entire margin, which disappeared 30 min later, marking the first cycle of the segmentation clock (Fig. 3B and fig. S1) (*13*). Hence, the clock's initiation coincides with, or shortly precedes, the inferred onset of desynchronization, and initial synchrony among these genetic oscillators appears to be achieved by simultaneous gene induction.

Three more oscillatory cycles were found confined to the ring of the gastrulating mesoderm with an interval between maximum expression states of around 30 min, corresponding to the period of the segmentation clock (Fig. 3C). During these cycles, *dlc* expression started at the ventral side of the embryonic margin and moved dorsally, thereby forming a traveling wave (Fig. 3, D and E). Furthermore, period seemed to decrease, whereas cellular expression levels increased, which is characteristic for transients following bifurcation events (*18*). During the subsequent fifth cycle, a cyclic expression domain separated from the gastrula margin at 8.2 hpf and moved anteriorly. The earliest previously reported wave at 8.7 hpf (*15*, *24*, *25*) marked the sixth cycle and prefigured the first segment boundary. These five cycles before somitogenesis in zebrafish contrast to two observed in chick (*26*). Thus, throughout development, four related spatiotemporal oscillation patterns of the zebrafish's segmentation clock are now distinguishable (Fig. 3F).

To test the requirement of intercellular Delta-Notch signaling for clock initiation, we subjected WT embryos to DAPT. The oscillating expression patterns of *dlc* at 65% epibioly were indistinguishable from those of WT (Fig. 3, G and H). In contrast, embryos injected with MOs targeting the *h/E(Spl)* genes *her1* and *her7*, jointly required for segmentation along the entire axis (*15*, *27*), showed sustained *dlc* expression (Fig. 3I), indicating loss of cyclic gene oscillations. Thus, the first synchronous oscillations of the segmentation clock require h/E(Spl) transcriptional repressors, but, consistent with the desynchronization hypothesis (*5*), we found no evidence for a Delta-Notch requirement.

Although the clock attains initial synchrony via simultaneous initiation of its oscillators, according to Eqs. 2 and 3 a coupling-dependent, self-organized synchronization over multiple periods among initially unsynchronized oscillators (*18*, *20*, *21*) should also be possible. Embryos subjected to a DAPT pulse from 4 to 15 hpf (Fig. 4A) showed an ALD of $S_{ALD} = 6.1 \pm 1.1$ ($N = 9$) (Fig. 4B) and concomitant, profound loss of synchrony in cells of the tailbud and presomitic mesoderm (PSM) evidenced by a disordered *dlc* expression pattern (Fig. 4, C to F), equivalent to that in Delta-Notch mutants (*5*, *15*, *28*, *29*). After DAPT washout, normal segment formation and cyclic gene expression was recovered (Fig. 4, B to G). The position of the last defective segment defines a posterior limit of defects (PLD), which we estimated at $S_{PLD} = 23.2 \pm 2.1$ (~21 hpf), indicating a recovery time of ~10 oscillation periods. Thus, restoration of Notch coupling is sufficient for self-organized resynchronization (*18*, *20*, *21*) of these previously desynchronized genetic oscillators, whereby both decay and recovery processes can be represented as a trajectory in a synchrony-coupling phase diagram (Fig. 4H, top).

We have demonstrated two general mechanisms by which genetic oscillators can attain synchrony: (i) simultaneous induction and (ii) self-organized synchronization, which, in the case of the segmentation clock, were Notch-independent and Notch-dependent, respectively. Delta-Notch mutant zebrafish embryos would allow screening for compounds restoring Delta-Notch coupling (*30*), with potential therapeutic implications for human genetic mal-segmentation disorders (*31*). These Delta-Notch mutant phenotypes are now quantitatively understandable from the desynchronization hypothesis (*5*) in terms of the decay rate λ, that is, the difference in noise, $2\sigma^2$, and coupling strength, ε (Eq. 3 and Fig. 4H, bottom), which determines the segmentation defect position. From the lowest ALD observed (Eq. 6) and assuming alternative coupling pathways negligible ($A = 0$), we estimate the clock's noise of $2\sigma^2 \approx 0.8\ hour^{-1}$, consistent with our estimates of noise (*13*) stemming from cell movements (*5*) and genetic sources. The system's robustness R (Eq. 9) then gives the WT Notch coupling strength of $\varepsilon_{WT} = R{\cdot}2\sigma^2 \approx 4\ hour^{-1}$. Thus, by using quantitative techniques for perturbation of gene function in combination with a physical theory of coupled phase oscillators, we were able to determine the essential dynamical properties that quantitatively account for a collective, morphological process in a complex developmental system.

References and Notes

1. J. Cooke, E. C. Zeeman, *J. Theor. Biol.* **58**, 455 (1976).
2. I. Palmeirim, D. Henrique, D. Ish-Horowicz, O. Pourquie, *Cell* **91**, 639 (1997).
3. K. Horikawa, K. Ishimatsu, E. Yoshimoto, S. Kondo, H. Takeda, *Nature* **441**, 719 (2006).
4. Y. Masamizu *et al.*, *Proc. Natl. Acad. Sci. U.S.A.* **103**, 1313 (2006).
5. Y. J. Jiang *et al.*, *Nature* **408**, 475 (2000).
6. S. A. Holley, R. Geisler, C. Nusslein-Volhard, *Genes Dev.* **14**, 1678 (2000).
7. S. A. Holley, D. Julich, G. J. Rauch, R. Geisler, C. Nusslein-Volhard, *Development* **129**, 1175 (2002).
8. M. Itoh *et al.*, *Dev. Cell* **4**, 67 (2003).
9. D. Julich *et al.*, *Dev. Biol.* **286**, 391 (2005).
10. A. C. Oates, C. Mueller, R. K. Ho, *Dev. Biol.* **280**, 133 (2005).
11. F. J. van Eeden *et al.*, *Development* **123**, 153 (1996).
12. S. A. Holley, *Genes Dev.* **20**, 1831 (2006).
13. Materials and methods are available on *Science* Online.
14. A. Geling, H. Steiner, M. Willem, L. Bally-Cuif, C. Haass, *EMBO Rep.* **3**, 688 (2002).
15. A. C. Oates, R. K. Ho, *Development* **129**, 2929 (2002).
16. M. Deniziak *et al.*, *Exp. Cell Res.* **313**, 156 (2007).
17. J. Westin, M. Lardelli, *Dev. Genes Evol.* **207**, 51 (1997).
18. A. Pikovsky, M. Rosenblum, J. Kurths, *Synchronization: A Universal Concept in Nonlinear Sciences*, Cambridge Nonlinear Science Series (Cambridge Univ. Press, Cambridge, 2003).
19. J. Lewis, *Curr. Biol.* **13**, 1398 (2003).
20. A. T. Winfree, *Science* **298**, 2336 (2002).
21. J. Garcia-Ojalvo, M. B. Elowitz, S. H. Strogatz, *Proc. Natl. Acad. Sci. U.S.A.* **101**, 10955 (2004).
22. N. Barkai, S. Leibler, *Nature* **387**, 913 (1997).
23. G. Forgacs, S. Newman, *Biological Physics of the Developing Embryo* (Cambridge Univ. Press, Cambridge, 2005).
24. M. Muller, E. v Weizsacker, J. A. Campos-Ortega, *Development* **122**, 2071 (1996).
25. L. Smithers, C. Haddon, Y. Jiang, J. Lewis, *Mech. Dev.* **90**, 119 (2000).
26. C. Jouve, T. Iimura, O. Pourquie, *Development* **129**, 1107 (2002).
27. C. A. Henry *et al.*, *Development* **129**, 3693 (2002).
28. S. S. Shankaran *et al.*, *Dev. Biol.* **304**, 615 (2007).
29. F. van Eeden, S. Holley, P. Haffter, C. Nusslein-Volhard, *Dev. Genet.* **23**, 65 (1998).
30. R. T. Peterson *et al.*, *Nat. Biotechnol.* **22**, 595 (2004).
31. O. Pourquie, K. Kusumi, *Clin. Genet.* **60**, 409 (2001).
32. A. Sawada *et al.*, *Development* **128**, 4873 (2001).
33. G. Weinmaster, C. Kintner, *Annu. Rev. Cell Dev. Biol.* **19**, 367 (2003).

34. We thank the MPI-CBG fish facility; S. Ares, L. Morelli, C.-P. Heisenberg, I. Rohde, I.-M. Tolic, F. Paluch, Z. Stardust, and members of the Oates and Laurent lab for ideas and critical comments; Zebrafish International Resource Center for cb1045 plasmid; and J. Howard, G. Laurent, a Della Martin fellowship, the Beckman foundation, and D. Kruse for support of I.H.R.-K. We apologize to authors who were not cited because of space constraints. This work was supported by the Max Planck Society. Author contributions are as follows: I.H.R.-K. and A.C.O., project design, data analysis, and manuscript preparation; all authors, experiments; and I.H.R.-K., theory and fitting.

Supporting Online Material

www.sciencemag.org/cgi/content/full/1142538/DC1
Materials and Methods
SOM Text
Figs. S1 to S3
References

14 March 2007; accepted 2 August 2007
Published online 16 August 2007;
10.1126/science.1142538
Include this information when citing this paper.